Title	Formation of contacts between doped carbon nanotubes and aluminum electrodes
Author(s)	Jones, Sarah L. T.; Greer, James C.
Publication date	2013
Original citation	Jones, S. L. T. and Greer, J. C. (2013) 'Formation of contacts between doped carbon nanotubes and aluminum electrodes', Journal of Applied Physics, 114(15), 153709 (8pp). doi: 10.1063/1.4826262
Type of publication	Article (peer-reviewed)
Link to publisher's version	http://aip.scitation.org/doi/10.1063/1.4826262 http://dx.doi.org/10.1063/1.4826262 Access to the full text of the published version may require a subscription.
Rights	© 2013 AIP Publishing LLC. This article may be downloaded for personal use only. Any other use requires prior permission of the author and AIP Publishing. The following article appeared in Jones, S. L. T. and Greer, J. C. (2013) 'Formation of contacts between doped carbon nanotubes and aluminum electrodes', Journal of Applied Physics, 114(15), 153709 (8pp). doi: 10.1063/1.4826262 and may be found at http://aip.scitation.org/doi/10.1063/1.4826262
Item downloaded from	http://hdl.handle.net/10468/4721

University College Cork, Ireland
Coláiste na hOllscoile Corcaigh

Formation of contacts between doped carbon nanotubes and aluminum electrodes

Sarah L. T. Jones and James C. Greer

Formation of contacts between doped carbon nanotubes and aluminum electrodes

Sarah L. T. Jones and James C. Greer[a)]
Tyndall National Institute, University College Cork, Lee Maltings, Cork, Ireland

A theoretical study of the a semiconducting carbon nanotube (CNT) bonding to an aluminum electrode is presented using density functional theory to determine the electronic structure, and charge transport across the junction is studied using non-equilibrium Green's functions. The properties of CNT-metal junctions are of interest for optimizing metal-semiconductor junctions for Schottky barrier transistors and for the formation of Ohmic contacts for nanoelectronics. We first consider the properties of an undoped (16,0) CNT bonded to an aluminum electrode, including an analysis of metal induced gap states and examination of the surface dipole. The junction is then modified by introduction of substitutional dopants into the CNT using nitrogen and boron to form *n*- and *p*-type semiconductors, respectively, and the resulting impact of the doping on current transport across the junctions is calculated. As an alternative doping strategy, tetrathiafulvalene is introduced endohedrally and found to act as an *n*-type dopant in agreement with previous experimental studies. From electron transmission and current voltage characteristics, it is found that the doped junctions can be engineered to have much lower onset resistances relative to the undoped junction. It is found that the current-voltage characteristics display increased resistance for larger forward and reverse biases: For one polarity, the resistance increase is associated with the introduction of the CNT band gap into the voltage bias window, whereas for the opposing voltage polarity, the resistance increase is due to large charge carrier-substitutional dopant scattering. For the case of the endohedral doping scheme, it is found that the carrier-dopant scattering is effectively absent. © *2013 AIP Publishing LLC*. [http://dx.doi.org/10.1063/1.4826262]

I. INTRODUCTION

Many promising carbon nanotube (CNT) applications require that the CNT forms a contact with metal.[1–5] Formation of CNT-metal junctions may be classified as either side contacted or end contacted. In the side contact configuration, the CNT side wall is physisorbed to a metal,[6] while in the end contact configuration, an open end of the CNT directly bonds to the metal.[7] In this work, focus is placed on the end contact configuration, whereby the open end of a CNT is chemically bonded to a metal surface. The metal used in the contact can determine whether an Ohmic (linear current-voltage (IV) relationship) or Schottky (rectifying current-voltage characteristic) contact is formed. Theoretical and experimental results indicate that the metal's work function ϕ_m determines the nature of a contact[8] in the absence of interface states;[9] Ohmic contacts result when high ϕ_m metals are used conversely, a low ϕ_m is associated with Schottky contacts.[10] While consideration of ϕ_m provides some insight as a simple indicator of contact behaviour, the value of the work function alone cannot account for the more subtle aspects of contact formation, such as the atomistic interface structure and resultant charge transfer. Previously, tight binding molecular dynamics studies indicated the importance of understanding the detailed CNT-interface geometry by demonstrating that the positions on the CNT where Ni-C bonds formed dramatically impacted the CNT properties.[11,12]

The aluminum-pristine (i.e., undoped) CNT contact has previously been studied theoretically by Bai *et al.*,[13] Okada and Oshiyama,[14] Odbadrakh *et al.*,[15] and Gao *et al.*[16] The Okada study considers a side contact configuration, while Bai considers side and end contacts. The works of Odbadrakh and Gao study the end contact configuration exclusively, using structures similar to those considered in this work, however doping of the CNT is not considered in their studies. Their work highlights the importance of considering the metal induced gap states (MIGS) or regions of finite DOS in the gap of the semiconducting CNT which are induced upon contacting to a metal. If the CNT region used in calculations is too short, semi-conducting CNTs appear metallic due to the slowly decaying MIGS.

Substitutional doping by boron or nitrogen results in metallic CNTs[17–20] but also introduces new effects that must be considered. The electronic properties of intrinsically metallic CNTs degrade on incorporation of substitutional dopants,[21,22] and in addition, it is difficult to precisely control the doping levels within the CNT giving rise to dopant atom fluctuations[23] which impact on achieving reproducible electronic properties. As CNTs are hollow, it is also possible to incorporate dopants within the interior of the CNT, i.e., endohedral doping. Endohedral dopants, such as fullerenes,[24] metallocenes,[25] and organic molecules,[24,26–30] have been studied in the literature.

This work focuses on end contacts between aluminum and doped (16,0)-CNTs, previous reports for the end contact configuration consider smaller diameter, less experimentally

a)Electronic mail: jim.greer@tyndall.ie

relevant CNTs. Idealized nitrogen and boron doped CNTs (i.e., we assume no additional defects) are considered for p- and n-type doping, respectively, along with the endohedral dopant tetrathiafulvalene (TTF) which is known to induce n-type doping in CNTs and is stable in atmosphere.[29] To the best of our knowledge, this work is the first computational study of doped CNTs bonded to metal contacts. In the following, the electronic structure of the junctions is examined using density functional calculations. The electronic transport properties of the junctions are considered using zero (linear response) and finite source-drain bias voltages; the latter is achieved by calculating the electron transmission using first principles non-equilibrium Green's function (NEGF) methods to determine IV characteristics for the junctions.

II. METHODS

Density functional theory (DFT) in conjunction with the NEGF formalism[31] as implemented in the OpenMX software package[32] is used to calculate the transport properties for the Al-CNT junctions. All calculations use the PBE[33] approximation to the generalised gradient approximation (GGA) exchange and correlation functional, along with normconserving pseudopotentials.[34] The Al-CNT interface is modelled by bonding a (16,0)-CNT (pristine; substitutionally doped with N and B; and endohedrally doped with TTF) to a (111) Al slab. In each case, the atomic positions are allowed to relax to minimize the total energy of the system, with the exception of the atomic positions of the Al back plane, which are held fixed during the optimization procedure. For the repeat units used to build the Al and CNT regions, the geometry optimization is performed until all forces are less than 5×10^{-4} Hartree/Bohr. The OpenMX code employs a linear combination of pseudo-atomic orbitals method,[35,36] the pseudo-atomic orbitals chosen in this work for the geometry optimizations are listed in Table I. An energy cut-off of 150 Ry is used for numeric integration and supercells were chosen such that there was a minimum vacuum of 1 nm in all non-periodic directions.

The NEGF method is used to study the electron transport properties of the CNT-Al junctions. In this approximation, the CNT and Al contacts are treated as semi-infinite regions described by electrode or "lead" self-energies, and

TABLE I. Basis sets used for geometry optimisations and NEGF calculations. The first part of the basis set notation, i.e., preceding the angular momentum designation (s, p) is the cut-off radius of the PAO in Bohr, the second part indicates the number of orbitals used for the valence electrons. For example, S 6.0-s2p2 implies a cut-off of 6.0 Bohr and a total of eight basis functions (2 s functions and 6p functions).

Element	Geometry	NEGF
H	4.0-s2	4.0-s2
B	4.5-s2p2	4.5-s1p1
C	4.5-s2p2	4.5-s2p1
N	4.5-s2p2	4.5-s1p1
Al	6.0-s2p3	6.0-s1p2
S	6.0-s2p2	6.0-s2p2

the central junction region is treated as a scattering region. The basis sets used in the NEGF calculations are as given in Table I. A $128 \times 128 \times 128$ grid is used for numeric integration and the cell size is again chosen to have 1 nm of vacuum in directions perpendicular to the transport direction. The calculations are considered converged when the norm of the residual density matrix was below at least 10^{-4} and ideally below 10^{-6}, although this stricter convergence criterion has negligible impact on the calculated electronic properties. Transmission curves are obtained as follows: First, band structure calculations are performed for the left (Al) and right (CNT) leads using the same basis sets to be employed in the subsequent NEGF calculations to generate a set of lead Hamiltonians; next NEGF calculations are performed for structures consisting of these leads and the central scattering region; finally NEGF results are used to calculate the electron transmission with the TranMain code. As well as calculating transmission at zero bias, we calculate the transmission at finite source-drain voltages across the junction. In the case of the pristine CNT, a full NEGF calculation is performed with increments of 0.1 V between -1.0 V and 1.0 V. We then use an interpolation scheme included in the TranMain code; the interpolation avoids the recalculation of the self-consistent Hamiltonian at each new voltage bias by a linear mixing as a function of the voltage of the Hamiltonian matrix elements to obtain estimates for intermediate bias values. Here, the interpolation scheme was used between zero bias and 1 V, and zero bias and -1 V to generate the same set of data points calculated from the explicit NEGF calculations. These interpolated values were used to assess the accuracy of the interpolation scheme for the subsequent studies of the Al-CNT systems, with good agreement found between the full NEGF and interpolated results (Figure S1[37]). For all other Al-CNT interfaces, full NEGF calculations are performed for 0 bias, 1 V and -1 V with interpolation used to generate additional data points. For each system studied, we check the validity of the interpolation by performing full NEGF calculations at two additional data points within the interpolated range to ensure difference in calculated currents between the full NEGF calculation and the interpolated version currents at the same voltages differ by less than a few percent.

III. ELECTRONIC STRUCTURE OF THE CNT LEADS

The structures of the CNT lead unit principle layers are shown in Figure 1. The undoped or pristine CNT lead consists of single repeat unit of the (16,0)-CNT unit cell containing 64 carbon atoms. The N- and B-doped leads consist of three repeat units of the pristine CNT lead cell with two substitutional dopants with the placement of the impurity atoms the same for p- and n-type doping. The substitutional dopant concentration is 1 at. %, a relatively low level for N- and B-dopants in CNTs whereby experimental doping levels can range up to 20 at. %. The TTF@CNT structure contains a single TTF molecule per unit cell of the (16,0)-CNT; this dopant concentration has been previously reported by Lu $et\ al.$[28] and found to be necessary for the doping of the CNT by the encapsulated TTF to be observed. The TTF@CNT
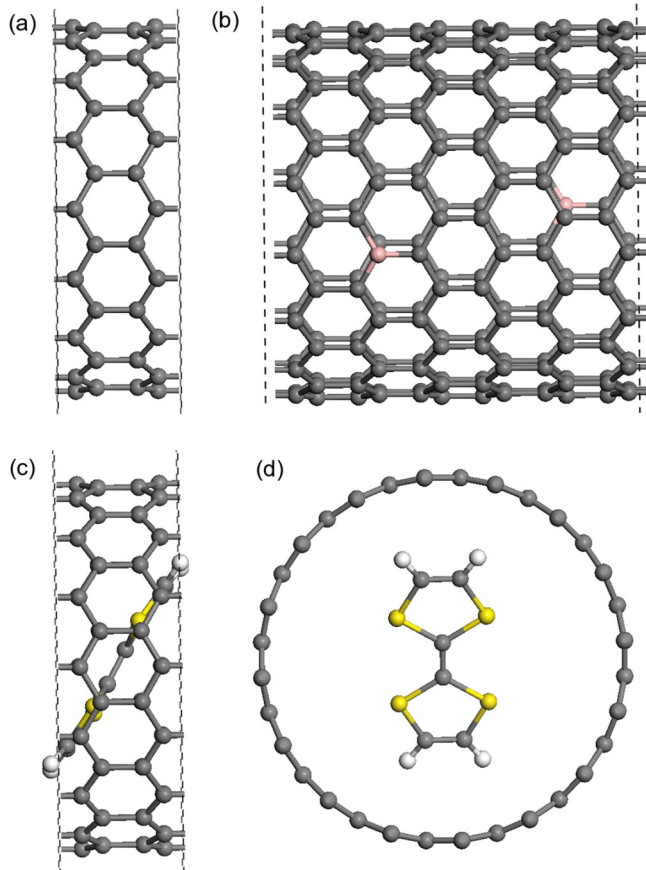
FIG. 1. Optimized (16,0)-CNT lead structures (carbon is grey, hydrogen is white, boron is pink, sulfur is yellow). (a) Side view of pristine (16,0)-CNT lead. (b) Side view of B-CNT lead (an identical dopant profile is used in the N-doped lead). Side (c) and top (d) view of TTF@CNT lead.

lead repeat unit used for transport calculations consists of three such unit cells; this was found to be necessary to avoid interaction between next nearest neighbor lead cells. Mulliken population's analysis shows that TTF donates electronic charge to the CNT as anticipated for an endohedral dopant with a small ionization energy. The encapsulated TTF molecules are found to have a net positive charge of $0.09 |e|$, hence $-0.09 |e|$ charge is contributed to the CNT, in reasonable agreement with the value of $0.12 |e|$ estimated by Lu et al.[28] and well within the error inherent in Mulliken population analysis.

The band structures of the CNT-lead regions are displayed in Figure 2. The pristine (16,0)-CNT has a calculated band gap of ~ 0.5 eV, which is consistent with literature DFT values for this chirality.[38] Even at the relatively low substitutional doping concentration for CNTs used in this study, the B-doped and N-doped band structures clearly show that the CNT becomes metallic following introduction of substitutional dopants with energy bands crossing the Fermi level. The bands corresponding to the pristine CNT persist but the gap is narrowed by approximately 0.1 eV and shifted to higher (lower) energies by ~ 0.5 eV for B-(N-)dopants. These findings are consistent with previous literature reports.[21,39,40] The band structure of TTF@CNT is consistent with n-type doping of the CNT, the flat dopant band meets the conduction band of the CNT close to the Fermi level.

This flat dopant bands contrast with the dopant bands with larger curvature seen for the introduction of B and N dopants, and imply that the TTF molecular states are localized with little interaction between endohedral dopants. This difference is consistent with the fact that the nitrogen and boron atoms are covalently bonded into the CNT sidewall, while the endohedral dopants are physisorbed inside the CNT. The study by Lu et al. finds a relatively curved dopant band for TTF@CNT when there is a single TTF molecule per CNT unit cell and conversely finds an almost flat band when there is a single TTF molecule per two CNT unit cells. The origin of the discrepancy between the two sets of band structures in the case of TTF is currently not known.

While the introduction of B and N in the CNT lattice clearly results in doping of the CNTs as is seen in the band structures in Figure 2, these dopant atoms also act as defects in the CNT lattice. Before considering the effect of forming a junction by contacting the CNTs to an aluminum lead, the scattering which results from the substitutional dopant atoms is assessed by considering the transmission across periodic CNT structures, with the results shown in Figure 3. At negative energies, a considerable deviation relative to the undoped CNT stepped transmission is seen for the B-doped CNT, and similarly at positive energies, a deviation is seen for the N-doped CNT. Therefore, significant electron scattering occurs when B and N dopants are incorporated into the CNT lattice, particularly in the valence band for B-doping and in the conduction band for N-doping. The dopant levels considered here are in at the lower end of the range of doping concentrations typically achieved in experiment; a greater reduction in the charge carrier transmission would be anticipated at higher doping levels. In the case of TTF@CNT, to a good approximation, the carrier transmission is only shifted relative to the pristine CNT (as would be expected from the band structures) without the introduction of significant scattering. The preservation of the ideal CNT lattice and resultant lack of scattering suggests that endohedral doping is an attractive alternative for doping of CNTs for electronic applications.

IV. Al-CNT INTERFACES

The junction used in the transmission calculations is shown in Figure 4 for the interface between Al and the pristine CNT. A similar structure is used for the calculations involving the doped CNT leads. For the carbon region, there are a total of seven CNT unit cells in the extended scattering region. In the electronic structure for the CNT bonded to the aluminum lead, a significant density of MIGS is found in the band gap of the CNT near the interface. The CNT unit cell bonded directly to the Al surface is labeled as "Repeat 1" in the inset of Figure 5(a) with the subsequent cells similarly labeled. The MIGS are found to drop off exponentially in Figure 5(a), with a low density of MIGS found after repeat cell 7 ("Repeat 7"). This result is consistent with that previously reported by Odbadrakh et al. for the interface between (8,0)-CNT and an Al electrode[15] and highlights the importance of considering sufficiently large structures in NEGF calculations for any metal-semiconducting CNT interfaces. The study of Al-CNT and Pd-CNT interfaces by Gao et al.[16]
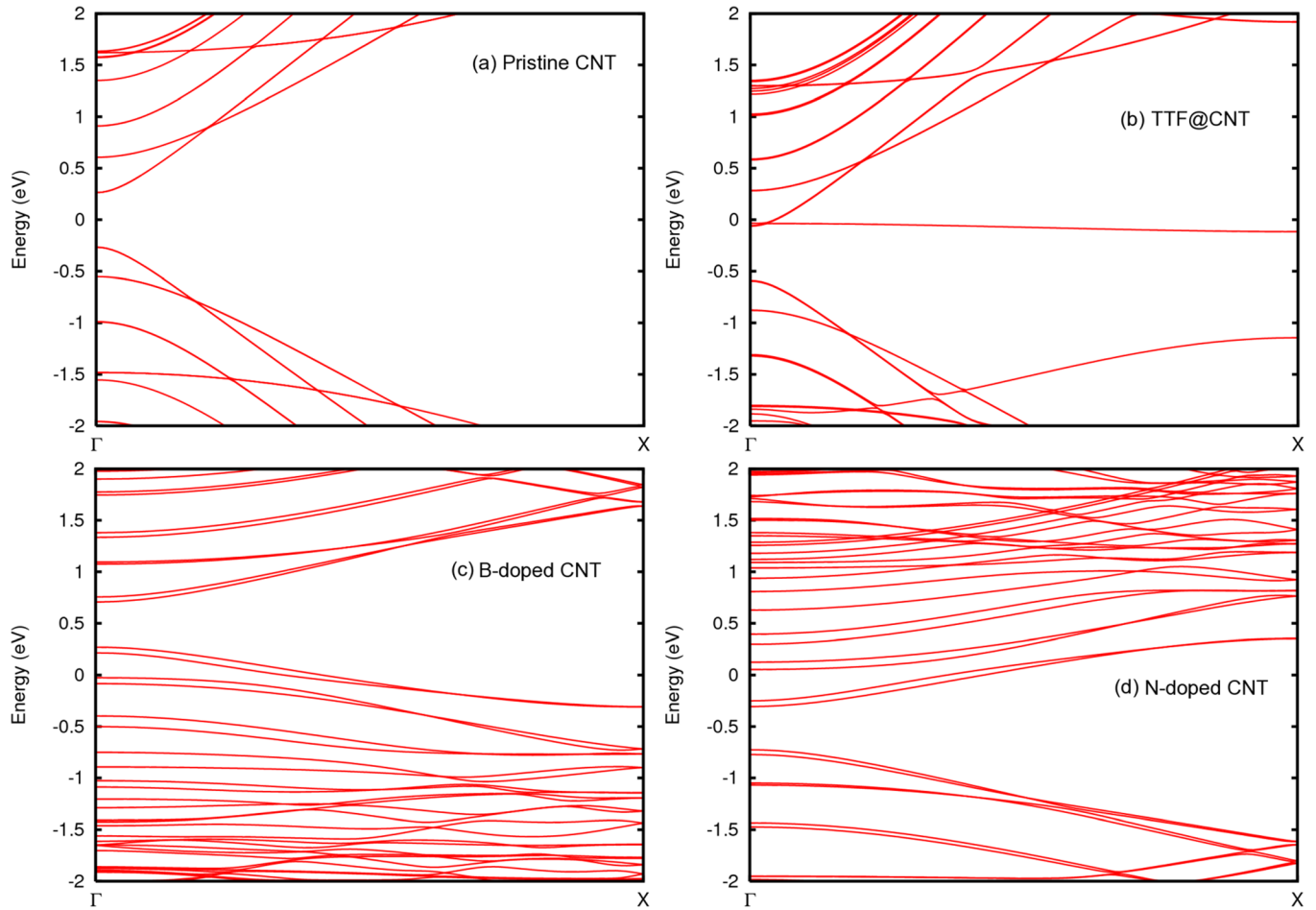
FIG. 2. Band structures for the pristine and doped (16,0)-CNT lead structures. The Fermi level is set to 0 eV in all cases.

introduces only two CNT cells between metal leads, consequently although the semi-conducting (10,0)-CNT was studied, they found no gap in transmission and therefore an Ohmic contact for an undoped CNT. Similarly for the doped CNT-metal interface, a penetration of MIGS is seen into semiconducting region, with the difference that the CNT energy gap is displaced relative to the Fermi energy as seen from the doped CNT lead band structures.

Figure 5(b) plots the average charge found on the atoms in the repeat cells of the structure in Figure 4 as determined by Mulliken population analysis indicating charge transfer from the Al nanowire to the CNT, i.e., a surface dipole forms with a total of 2.9 electrons donated to the CNT. A similar direction of charge transfer is found for the interfaces between Al and the doped CNT structures, with a transfer of $2.5\,|e|$, $1.6\,|e|$ and $1.5\,|e|$ found for
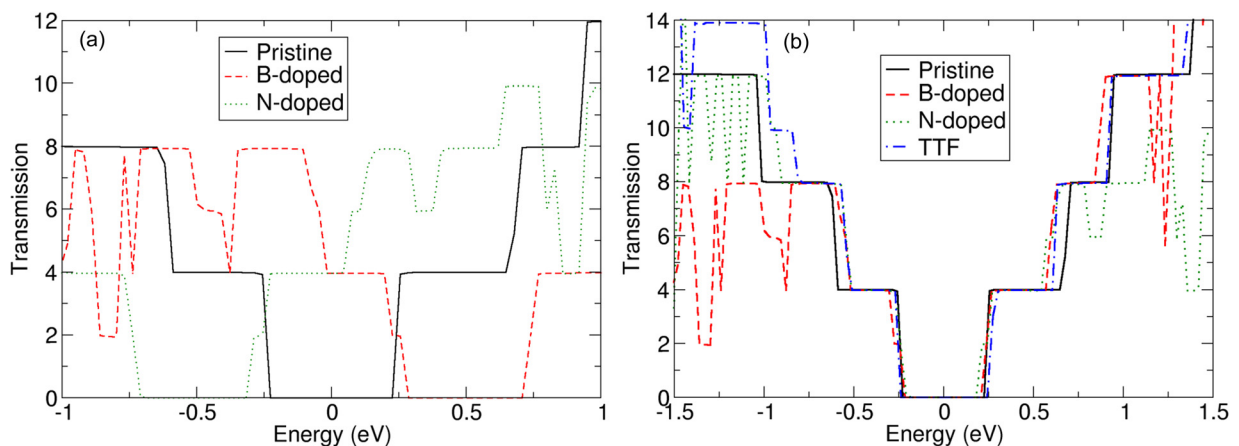

FIG. 3. Electron transmission for the doped CNTs. (a) The Fermi level is energy is set to 0 eV for all CNTs, the TTF@CNT curve is only shifted down in energy by ~0.35 eV relative to the pristine CNT and has been omitted for clarity. (b) The transmission spectra of the doped CNTs have been shifted to coincide with the transmission gap of the pristine CNT, to emphasize the scattering relative to the pristine CNT.

the B-doped CNT, N-doped CNT, and TTF@CNT, respectively.

In Figure 6, the transmission for the interface between the junction formed from the pristine CNT and Al at zero bias and selected negative and positive source drain biases are given. The zero-bias transmission matches up with the DOS plotted in the inset of Figure 5(a) as is expected, with no transmission for regions corresponding to energies with no DOS. The overall magnitudes of the transmission are lower for the CNT-metal junction than that of the CNT only
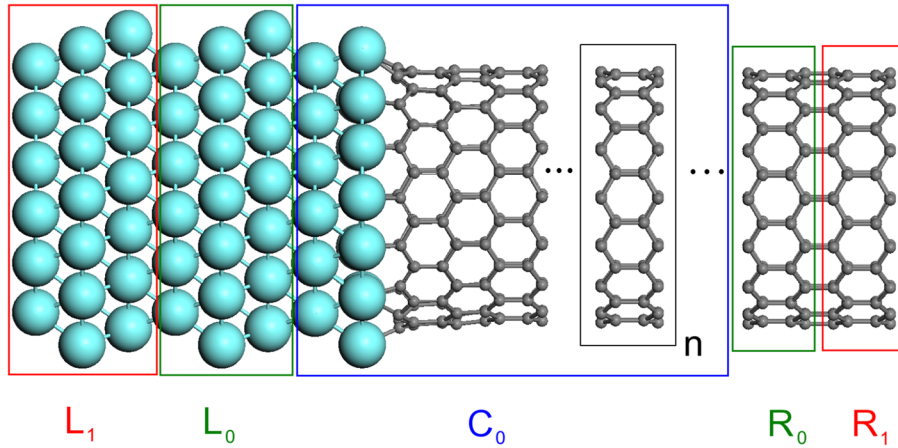

FIG. 4. Model structure for the Al-pristine CNT interface ($n = 4$). This structure also serves as the starting point for generating the junctions formed between Al and the doped CNTs. The regions R_1 and L_1 are used to build the electrode self-energies to describe the electrodes. $L_0 + C_0 + R_0$ make up the central region "C," the extended scattering region. Five layers of Al are computed explicitly.
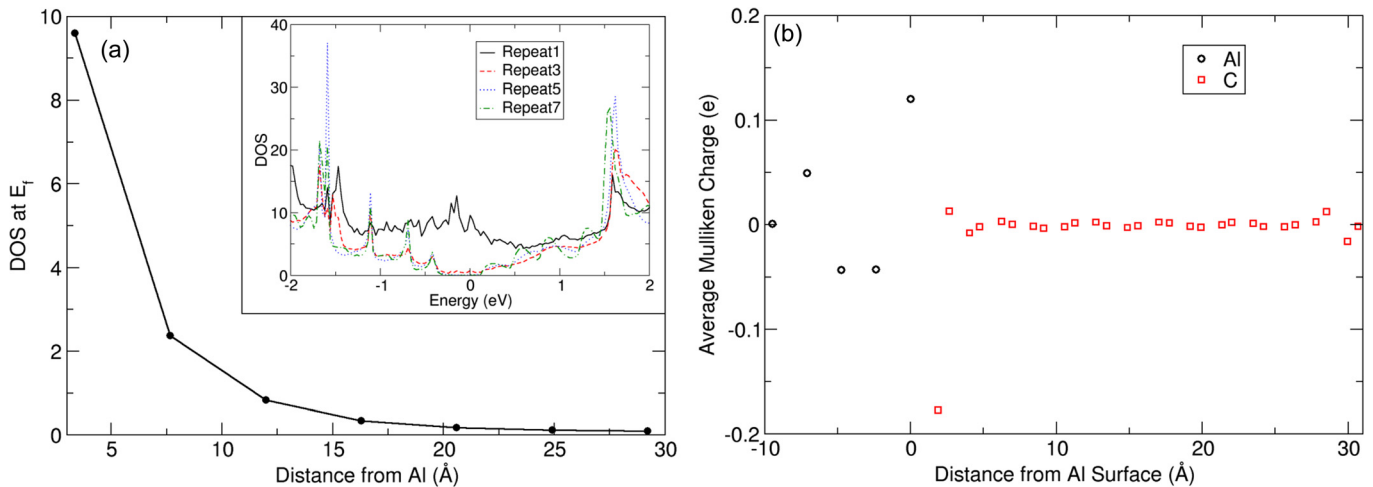

FIG. 5. (a) Decay of the MIGS at the Fermi energy with distance from the interface. (Inset): DOS of selected CNT repeat unit in the scattering region of the pristine CNT, note the reappearance of the CNT gap at larger distances. Plots for the doped CNTs are given in Figure S2.[37] (b) Average Mulliken charge per layer for the Al-CNT interface. Electronic charge is transferred from Al to carbon atoms at the interface.
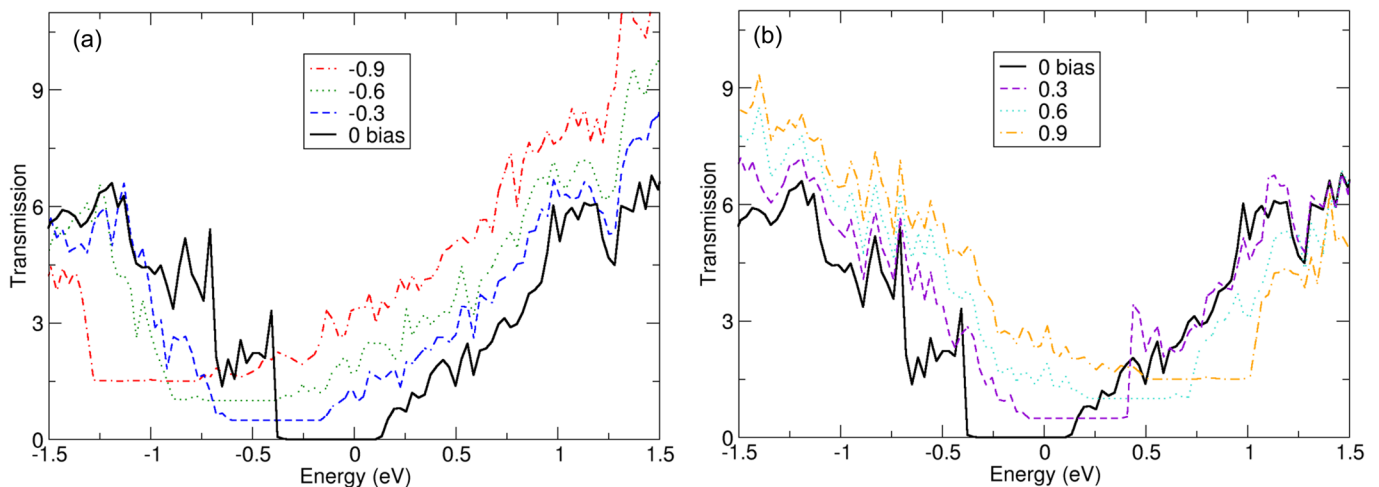

FIG. 6. Transmission of Al-pristine CNT interface for bias voltages for selected negative (a) and positive (b) source-drain bias voltages. The curves have been displaced along the y-axis for clarity.
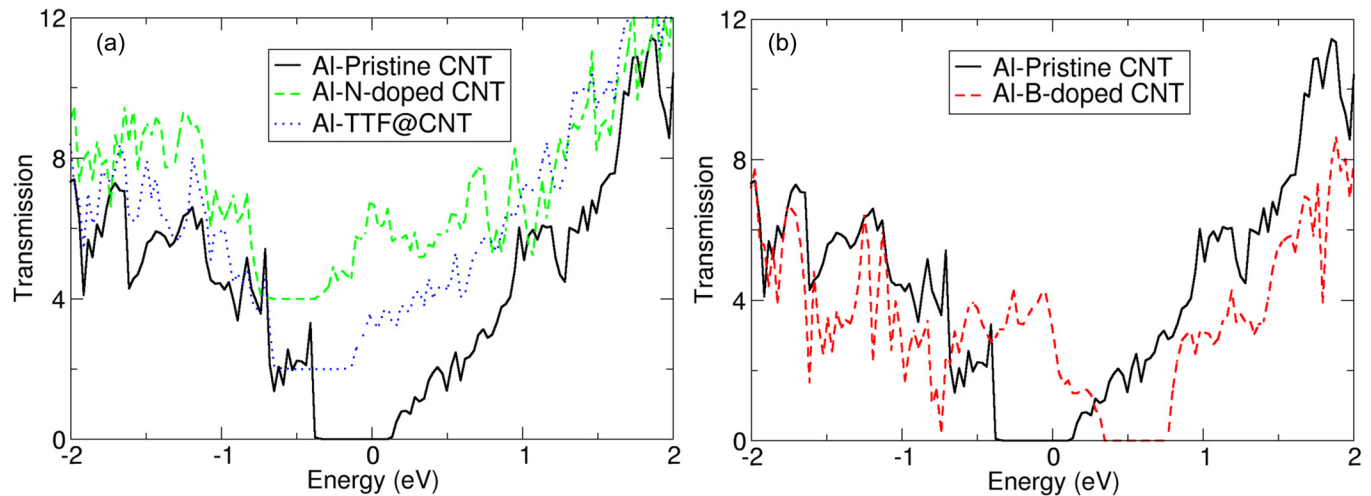
FIG. 7. (a) Transmission of the pristine, N-doped and TTF@CNT contacts with Al. For clarity, the transmissions of the doped interfaces have been shifted along the y-axis. (b) Transmission of the pristine and B-doped CNT interfaces.

structure (Figure 3) implying that significant electron scattering takes place at the interface. The primary affect of applying a source drain bias is to shift the obtained transmission, as shown in Figure 6. A negative applied bias pushes the Fermi energy above the transmission gap associated with the CNT, while a positive applied bias has the opposite effect, with the bias window moving below the region of zero transmission. The current can be related to an integral of the transmission as a function of energy over a voltage bias window. At zero applied bias, there is no current. As a negative bias is applied, the transmission becomes non-zero below -0.3 V as seen in Figure 6(a), therefore the current onset in the reverse direction is expected at this voltage. If positive voltage bias is applied, the transmission in Figure 6(b) becomes non-zero for forward applied voltages greater than 0.3 V, thus we can anticipate that the IV characteristic is asymmetric for the junction formed between the pristine CNT and Al nanowire.

Figure 7 plots the zero bias transmission for the pristine and doped CNT interfaces formed by bonding to the Al lead. The shifting and narrowing of the CNT gap seen due to doping with B and N are preserved when the CNT is contacted to metal. The magnitude of the (shifted) transmissions for the B- and N-doped contacts with Al is generally less than that of the pristine CNT/Al junction; the scattering which results from substitutional dopants has an impact and is visible in the transmission curve beyond that due to scattering at the metal-CNT interface. For example, there is a trough in transmission for the B-doped CNT interface at ~ -0.9 eV which corresponds to a similar trough in the transmission seen for the B-doped CNT lead (see Figure 3(a)), a similar sharp drop in transmission which can be attributed to scattering at the dopant atom can be seen at ~ 0.7 eV in the case of the N-doped CNT. Dopant introduced scattering sites in the CNT region clearly have an impact on the IV characteristics even upon formation of the metal-semiconductor junction. In the case of TTF, the transmission follows closely the transmission of the pristine CNT-Al interface once the relative shift in the Fermi level introduced upon doping is taken into

consideration, again illustrating that the endohedral dopant does not cause significant scattering because it does not disrupt the CNT lattice to the same extent as substitutional dopants.

The current-voltage characteristics of the pristine and substitutionally doped CNT-Al interfaces are shown in Figure 8. As previously indicated, there is no current through the pristine CNT-Al interface at low source-drain voltage biases and there is an asymmetric IV behaviour due to the Fermi level alignment being closer to the conduction band of the CNT. This is in contrast to the behavior of the junctions formed between the B- and N-doped CNTs and the Al lead. Similar IV curves are obtained for both p- and n-type substitutional dopants with a linear IV at low bias indicating an Ohmic contact is formed as suggested by the non-zero DOS at the Fermi level. The transmission gap due to the CNT band gap is encountered for the B-doped CNT/Al interface resulting in a plateau in the current as the voltage becomes increasingly negative. A similar behavior is seen for the N-doped interface for positive bias voltages. However, a
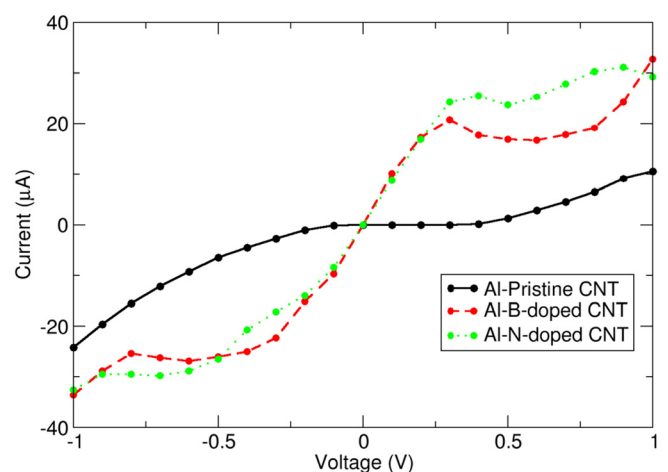

FIG. 8. Current-voltage characteristics of the pristine and doped Al-CNT interfaces.
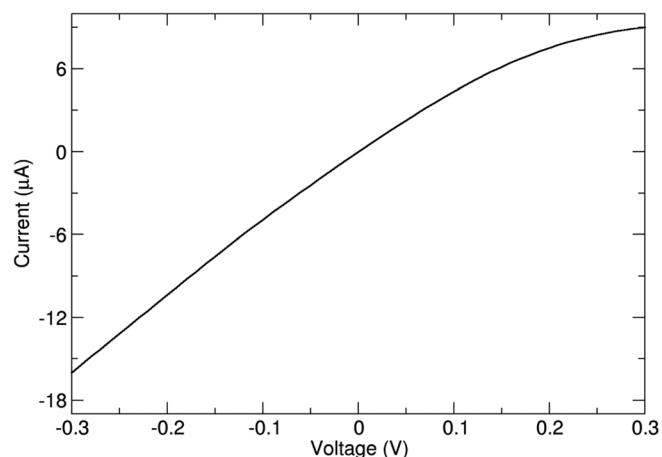
FIG. 9. Linear response IV curve for Al-TTF@CNT interface. Reasonable agreement is found between linear response and NEGF currents at low bias (Figure S3[37]).

flattening of the IV curve is also seen at large bias values for which the transmission gap does not enter into the bias window as can be seen in Figure 7 for both the B- and N-doped CNT/Al interfaces. For these voltage biases, the bias window spans the valence band for the *p*-type CNT and similarly the conduction band for the *n*-type CNT. The additional scattering introduced by the dopant atoms in these energy ranges increases the resistance of the junction resulting in a flattening of the current at larger voltage biases. However, the IV characteristics can be described as approximately Ohmic for lower voltage biases and the junction physics reduces the currents for larger negative and positive voltage bias. The increasing resistance at larger voltages is due to two different mechanisms: For one polarity, it arises from the transmission gap entering into the voltage bias window and for the opposing polarity it is due to increased scattering arising from the voltage bias window encompassing a doped bands. As can be seen in the Figure 8, these two distinct mechanisms result in similar levels of current reduction for the approximate voltage ranges of ± 0.5 to ± 1.0 V.

In Figure 9, the linear response IV curve for the Al-TTF@CNT interface obtained from the zero-bias transmission results of Figure 7(a) is shown. At very low biases, the IV curve is linear and at negative applied bias this linearity is maintained. However, at a small positive bias of 0.1 V, the IV curve begins to flatten as the CNT transmission gap is encountered in an analogous fashion to the interface with the N-doped CNT, though at a lower bias (see Figures 7(a) and 8). As already discussed, endohedral TTF dopes the CNT with minimal scattering, therefore it can also be anticipated that even at higher applied negative biases, the IV will remain linear. Thus, the contact has a diode-like behaviour. At positive applied biases, the CNT gap is encountered at low bias (<200 mV) and the current saturates at $\sim 8\,\mu$A, while at negative biases, a linear current-voltage relationship is maintained.

V. CONCLUSION

The electronic structure properties of doped (16,0)-CNTs and CNT-Al contacts have been studied for substitutional *p*- and *n*-type doping, and for endohedral *n*-type

molecular doping. It is found that substitutional doping by boron and nitrogen at concentrations of 1 at. % makes the (16,0)-CNT metallic. Following junction formation between the CNT with an Al lead, the presence of MIGS has been identified and their penetration into the semiconducting CNT has been quantified; the resulting DOS in the CNT band gap can extend beyond 2 nm from the metal-semiconductor junction. Conversely, the surface dipole formed at the metal-semiconductor junction due to charge transfer at the surface bonds is localized directly at the interface with the regions of positive and negative charges extending only over a region of approximately 0.5 nm.

A slightly asymmetric IV curve occurs for the Al-contacted undoped CNT with little current at low source-drain biases. For the Al-contacted B- and N-doped CNTs, similar IV characteristics are found, with an Ohmic behavior occurring at low bias. However at larger biases, the IV curve becomes non-linear because the shifted CNT gap is encountered and due to scattering off the B/N atoms in the CNT, depending on the voltage polarity. Similarly, for endohedral doping using the TTF molecule, the IV characteristic is approximately Ohmic for small voltages. In the reverse bias direction, there is in an approximately linear IV curve relative to the case of N substitutional doping, revealing that the endohedral dopants do not introduce significant scattering. Our calculations confirm that conventional doping strategies can be applied in the engineering of CNT-metal junctions, indicating that Ohmic junctions can be engineered for CNT-metal contacts. Additionally, it is found that the use of endohedral doping can achieve similar transport properties at low voltage biases without introducing significant dopant scattering into the CNT for higher voltage biases.

ACKNOWLEDGMENTS

[1]S. J. Tans, A. R. M. Verschueren, and C. Dekker, Nature **393**, 49 (1998).
[2]A. Javey, H. Kim, M. Brink, Q. Wang, A. Ural, J. Guo, P. McIntyre, P. McEuen, M. Lundstrom, and H. Dai, Nature Mater. **1**, 241 (2002).
[3]R. Weitz, U. Zschieschang, F. Effenberger, H. Klauk, M. Burghard, and K. Kern, Nano Lett. **7**, 22 (2007).
[4]P. Avouris, Z. H. Chen, and V. Perebeinos, Nat. Nanotechnol. **2**, 605 (2007).
[5]G. F. Close, S. Yasuda, B. Paul, S. Fujita, and H. S. P. Wong, Nano Lett. **8**, 706 (2008).
[6]H. M. Manohara, E. W. Wong, E. Schlecht, B. D. Hunt, and P. H. Siegel, Nano Lett. **5**, 1469 (2005).
[7]C. Santini, A. Volodin, C. Van Haesendonck, S. De Gendt, G. Groeseneken, and P. M. Vereecken, Carbon **49**, 4004 (2011).
[8]W. G. Zhu and E. Kaxiras, Nano Lett. **6**, 1415 (2006).
[9]J. Svensson and E. E. B. Campbell, J. Appl. Phys. **110**, 111101 (2011).
[10]F. Leonard and J. Tersoff, Phys. Rev. Lett. **84**, 4693 (2000).
[11]A. N. Andriotis, M. Menon, and G. E. Froudakis, Appl. Phys. Lett. **76**, 3890 (2000).
[12]A. N. Andriotis, M. Menon, and G. E. Froudakis, Chem. Phys. Lett. **320**, 425 (2000).

[13]P. Bai, E. Li, K. T. Lam, O. Kurniawan, and W. S. Koh, Nanotechnology **19**, 115203 (2008).

[14]S. Okada and A. Oshiyama, Phys. Rev. Lett. **95**, 206804 (2005).

[15]K. Odbadrakh, P. Pomorski, and C. Roland, Phys. Rev. B **73**, 233402 (2006).

[16]F. Gao, J. M. Qu, and M. Yao, J. Electron. Packag. **133**, 020908 (2011).

[17]K. Liu, P. Avouris, and R. Martel, Phys. Rev. B **63**, 161404 (2001).

[18]J. A. Talla, Physica B **407**, 966 (2012).

[19]S. H. Lim, R. Li, W. Ji, and J. Lin, Phys. Rev. B **76**, 195406 (2007).

[20]A. C. M. Carvalho and M. C. dos Santos, J. Appl. Phys. **100**, 084305 (2006).

[21]C.-C. Kaun, B. Larade, H. Mehrez, J. Taylor, and H. Guo, Phys. Rev. B **65**, 205416 (2002).

[22]S. Latil, S. Roche, D. Mayou, and J.-C. Charlier, Phys. Rev. Lett. **92**, 256805 (2004).

[23]W. K. Hsu, S. Firth, P. Redlich, M. Terrones, H. Terrones, Y. Q. Zhu, N. Grobert, A. Schilder, R. J. H. Clark, H. Q. Kroto, and D. R. M. Walton, Mater. Chem. **10**, 1425 (2000).

[24]W. Z. Liang, J. L. Yang, and J. Sun, Appl. Phys. Lett. **86**, 223113 (2005).

[25]L. J. Li, A. N. Khlobystov, J. G. Wiltshire, G. A. D. Briggs, and R. J. Nicholas, Nature Mater. **4**, 481 (2005).

[26]V. Meunier and B. G. Sumpter, J. Chem. Phys. **123**, 024705 (2005).

[27]J. Lu, S. Nagese, X. W. Zhang, D. Wang, M. Ni, Y. Maeda, T. Wakahara, T. Nakahodo, T. Tsuchiya, T. Akasaka, Z. X. Gao, D. P. Yu, H. Q. Ye, W. N. Mei, and Y. S. Zhou, J. Am. Chem. Soc. **128**, 5114 (2006).

[28]J. Lu, S. Nagese, D. P. Yu, H. Q. Ye, R. S. Han, Z. X. Gao, S. Zhang, and L. M. Peng, Phys. Rev. Lett. **93**, 116804 (2004).

[29]T. Takenobu, T. Takano, M. Shiraishi, Y. Murakami, M. Ata, K. Katuara, Y. Achiba, and Y. Iwasa, Nature Mater. **2**, 683 (2003).

[30]R. G. A. Veiga and R. H. Miwa, Phys. Rev. B **73**, 245422 (2006).

[31]T. Ozaki, K. Nishio, and H. Kino, Phys. Rev. B **81**, 035116 (2010).

[32]See http://www.openmx-square.org/ for access to the open source numerical atomic orbital DFT code OpenMX.

[33]J. P. Perdew, K. Burke, and M. Ernzerhof, Phys. Rev. Lett. **77**, 3865 (1996).

[34]I. Morrison, D. M. Bylander, and L. Kleinman, Phys. Rev. B **47**, 6728 (1993).

[35]T. Ozaki, Phys. Rev. B **67**, 155108 (2003).

[36]T. Ozaki and H. Kino, Phys. Rev. B **69**, 195113 (2004).

[37]See supplementary material at http://dx.doi.org/10.1063/1.4826262 for additional Figures: (S1) comparison of NEGF and interpolation scheme calculations for transport characteristics of the interface between Al and the undoped CNT, (S2) DOS showing MIGS for the interfaces involving the doped CNTs, and (S3) comparison of NEGF and linear response IV characteristics for the Al-B-doped CNT interface.

[38]V. Zólyomi and J. Kürti, Phys. Rev. B **70**, 085403 (2004).

[39]A. M. Nemilentsau, M. V. Shuba, G. Y. Slepyan, P. P. Juzhit, S. A. Maksimenko, P. N. D'yachkov, and A. Lakhtaakia, Phys. Rev. B **82**, 235424 (2010).

[40]X. M. Liu, H. R. Gutierrez, and P. C. Eklund, J. Phys.: Condens. Matter **22**, 334213 (2010).